Natural Resources for Human Health
eISSN: 2583-1194

Original Research

Received 21 July 2026
Revised 30 Aug 2026
Accepted 14 Sep 2026

Natural Resources for Human Health 2026, Vol. 6 (21s): 77–94

KEYWORDS:
Vantex; gamma-cyhalothrin; pyrethroid; uterus; ovary; hemomicrocirculatory bed; Ki-67; Bcl-2; postnatal morphogenesis; developmental reproductive toxicity; rat

Effects of Low Doses of Pesticides on the Hemomicrocirculatory Bed and Tissue Structures of the Uterus in Rats During Early Postnatal Ontogenesis

Saulekhan Xojanazarova Jubatirovna[1], Zumrat Sodikhova Shavkatovna[2], Gulnora Islamova Raufovna[3], Azamat Nortaev Begmatovich[4], Norbek Niyozov Kurbonovich[5], Gulshakhnoza Muhammadieva Mamrajab qizi[6], Umerov Azimjon Abripi o‘g‘li[7], Djaxangirov Gayrat Xamdamovich[8], Maftuna Samatova Gulom qizi[9]

[1] Associate professor, Department of Human Anatomy and OCTA, Tashkent State Medical University, Tashkent, Uzbekistan. E-mail: saulexojanazarova70@gmail.com . ORCID: https://orcid.org/0000-0002-8892-5934
[2] Professor, Department of Human Anatomy and OCTA, Tashkent State Medical University, Tashkent, Uzbekistan. E-mail: sodikova.zumrat@inbox.ru . ORCID: https://orcid.org/0000-0001-6358-3766
[3] Associate professor, Department of Human Anatomy and OCTA, Tashkent State Medical University, Tashkent, Uzbekistan. E-mail: islamovag31@gmail.com . ORCID: https://orcid.org/0009-0001-1881-4710
[4] Assistant, Department of Human Anatomy and OCTA, Tashkent State Medical University, Tashkent, Uzbekistan. E-mail: azamatnortayev27@gmail.com . ORCID: https://orcid.org/0000-0002-3123-6169
[5] Department of Anatomy and Clinical Anatomy, Tashkent Medical Academy, Tashkent, Uzbekistan. E-mail: norbekniyozov65@gmail.com . ORCID: https://orcid.org/0009-0003-0071-3000
[6] Assistant Lecturer, Department of Human Anatomy, Operative Surgery and Topographic Anatomy, Tashkent State Medical University, Tashkent, Uzbekistan. E-mail: gulshakhnozalily@gmail.com . ORCID: https://orcid.org/0009-0009-3988-3270
[7] Assistant, Department of Human Anatomy and OCTA, Tashkent State Medical University, Tashkent, Uzbekistan. E-mail: umerovazimjon722@gmail.com . ORCID: https://orcid.org/0009-0000-1854-5621
[8] Lecturer, Department of Medical Biology, EMU University. E-mail: gayratjahongirovv@gmail.com . ORCID: https://orcid.org/0009-0009-9699-7266 3
[9]Assistant lecturer, Department of Public Health Nomer. 2, Tashkent State Medical University Tashkent, Uzbekistan E- mail: mubinasamatova97@gmail.com . ORCID: https://orcid.org/0009-0001-2756-7504

Highlights

Chronic low-dose maternal Vantex exposure disrupts postnatal utero-ovarian morphogenesis in rat offspring.

Microvascular change precedes parenchymal injury and is detectable from postnatal day 7.

Medullary venule lumen is widened approximately 1.3-fold at postnatal day 21.

The physiological postnatal expansion of the uterine venous bed is blunted after exposure.

Natural Resources for Human Health
eISSN: 2583-1194

Ki-67 and Bcl-2 upregulation reflects a compensatory response that does not restore architecture.

ABSTRACT: Background. Synthetic pyrethroids remain among the most widely applied insecticides in intensive agriculture. Vantex, a gamma-cyhalothrin formulation, combines high insecticidal potency with the capacity for transplacental and lactational transfer, which places the developing female reproductive tract at particular risk. The microvascular component of this injury has rarely been reconstructed morphologically.

Objective. To characterise postnatal morphogenesis of the hemomicrocirculatory bed and the tissue structures of the uterus and ovary in offspring born to dams with chronic low-dose Vantex intoxication, and to assess proliferative (Ki-67) and anti-apoptotic (Bcl-2) immunoreactivity.

Materials and methods. Outbred white rats were allocated to two groups of 30 dams each: intact controls and dams receiving Vantex at 4.0 mg/kg body weight per day by oral administration throughout gestation and lactation. Offspring were examined on postnatal days (PND) 7, 14, 21 and 30. Uterine angioarchitecture was visualised after infusion of Gerota mass through the abdominal aorta followed by clearing according to Sagatov. Paraffin sections 5–7 μm thick were stained with haematoxylin and eosin. Ki-67 and Bcl-2 were demonstrated with monoclonal antibodies on a Ventana BenchMark XT platform using 3,3′-diaminobenzidine chromogen. Evaluation was qualitative and semi-quantitative; no inferential statistical testing was performed.

Results. Maternal Vantex exposure produced inflammatory-destructive remodelling of utero-ovarian microvessels, condensation of stromal collagen and elastic fibres, premature atresia of centrally placed oocytes, thecal dystrophy, necrotic foci among luteocytes, and blunting of the physiological expansion of the uterine venous bed. Medullary venule lumen was approximately 1.3-fold wider than in controls by PND 21. Ki-67 labelling increased in isthmicocervical glandular epithelium and in ovarian parenchyma and stroma; Bcl-2 remained clearly positive at PND 30. Vascular change was detectable before overt parenchymal destruction.

Conclusions. In this mother–offspring model, Vantex behaves as a reproductive toxicant whose tissue injury is tightly coupled to failure of the hemomicrocirculatory bed. Juvenile morphological endpoints that include angioarchitecture deserve consideration in the assessment of modern pyrethroids, and preventive measures are warranted for populations with chronic pyrethroid exposure.

Abbreviations: DAB – 3,3′-diaminobenzidine; GSH – glutathione; H&E – haematoxylin and eosin; IHC – immunohistochemistry; JMPR – Joint FAO/WHO Meeting on Pesticide Residues; MDA – malondialdehyde; N/C – nuclear–cytoplasmic; NOAEL – no-observed-adverse-effect level; PND – postnatal day; SOD – superoxide dismutase; StAR – steroidogenic acute regulatory protein; 3β-HSD / 17β-HSD – 3β- and 17β-hydroxysteroid dehydrogenase.

1. INTRODUCTION

The continuing expansion of chemical plant protection keeps human contact with insecticides at a high level. Toxicological reviews estimate that global demand for pesticide products rises by several per cent annually and may approach multi-million-tonne volumes within the present decade [3,4]. Among current insecticide classes, synthetic pyrethroids occupy a dominant position because they combine high potency against target insects with comparatively low application rates and a favourable acute mammalian toxicity profile [5].

That favourable acute profile, however, says little about developmental outcomes. Type II pyrethroids act on voltage-gated sodium channels and interact with membrane lipids, and their neurotoxic mechanism is well characterised [17]. Beyond the

nervous system, the same physico-chemical properties make endothelium and actively differentiating epithelia plausible targets, and an expanding literature now treats pyrethroids as endocrine-active compounds rather than as narrowly neurotoxic agents [19,20].

Pregnant women, fetuses and neonates constitute particularly vulnerable cohorts. Adaptive reserves of anatomo-physiological systems are reduced during critical windows of ontogeny, and lipophilic residues cross the placenta and are secreted in milk [6,7]. Chronic exposure of women of reproductive age therefore has direct implications for the structural integrity of the offspring's reproductive organs [8,9].

Experimental work with lambda-cyhalothrin, the stereoisomeric relative of the gamma-cyhalothrin contained in Vantex, has shown ovarian oxidative stress, disrupted steroidogenesis, altered oestrous cyclicity and histopathological degeneration of follicles, with partial rescue by antioxidant supplementation [10–12,21]. Perinatal studies with the phenylpyrazole fipronil likewise demonstrate delayed vaginal opening and disturbed cyclicity in female rat offspring, confirming that contemporary insecticides can programme reproductive development even when gross malformations are absent [13,14].

What remains incomplete is the morphological reconstruction of the hemomicrocirculatory bed of the uterus and ovary during early postnatal life after maternal pyrethroid intoxication. Intra-organ vessels determine the trophic support of folliculogenesis and myometrial maturation, and vascular investment accompanies epithelial–mesenchymal interactions throughout differentiation of the female reproductive tract [15,16,24]. Microvascular failure may therefore be the proximate mechanism of delayed reproductive morphogenesis rather than a secondary epiphenomenon. Studies previously performed at Tashkent State Medical University established the present experimental model and showed that chronic maternal intoxication with Vantex impairs ovarian vascular–tissue remodelling and that uterine mural vessels undergo inflammatory-destructive change with secondary atrophy of tissue elements [1,2,25].

Aim of the study. To investigate morphological changes of the uterus and ovaries in offspring born under chronic toxic action of Vantex on the maternal organism, with particular emphasis on the hemomicrocirculatory bed, folliculogenesis, and the immunohistochemical markers Ki-67 and Bcl-2. The novelty of the present work lies in treating the microcirculatory bed as the primary organising endpoint and in reading proliferative and anti-apoptotic markers against that vascular background, rather than reporting them as independent findings.

2. MATERIALS AND METHODS

2.1. Animals and husbandry

Experiments were performed on mature white outbred female rats maintained under standard vivarium conditions with a controlled light–dark cycle, free access to water and balanced chow, and ambient temperature and humidity within institutional specifications. Animals were allocated to two groups of 30 dams each. Group 1 (control) comprised intact dams whose pups served as the morphological reference. Group 2 (experimental) comprised dams exposed to Vantex. Mating with intact males was timed by vaginal cytology.

2.2. Test substance, dose and route

Vantex is a last-generation pyrethroid insecticide of intestinal–contact action whose active principle is the single-isomer molecule gamma-cyhalothrin; it carries human hazard class 3 [2]. The formulation used was a commercial gamma-cyhalothrin product registered for agricultural use in Uzbekistan; the precursor publications do not record the manufacturer, the nominal content of active ingredient or the batch number, and this is noted among the limitations. Dams of Group 2 received the preparation at 4.0 mg/kg body weight per day by oral administration, daily and without interruption until the end of the experiment [2]. The dose was selected to reproduce the chronic regimen of the precursor experimental series rather than to approach an acute lethal fraction. It should be read against the regulatory reference values: the Joint FAO/WHO Meeting on Pesticide Residues sets a group acceptable daily intake of 0–0.02 mg/kg body weight and an acute reference dose of 0.02 mg/kg body weight for cyhalothrin and lambda-cyhalothrin [22]. The 4.0 mg/kg daily dose used here therefore exceeds the group acceptable daily intake by approximately 200-fold (Figure 1A) and is a deliberate experimental challenge, not a simulation of dietary intake. This distinction is important when the findings are extrapolated to human exposure, and it is revisited in Section 4.7. Where required by the chronic design, exposure continued through gestation and lactation, allowing both transplacental and lactational transfer of residual toxicant [7,13].

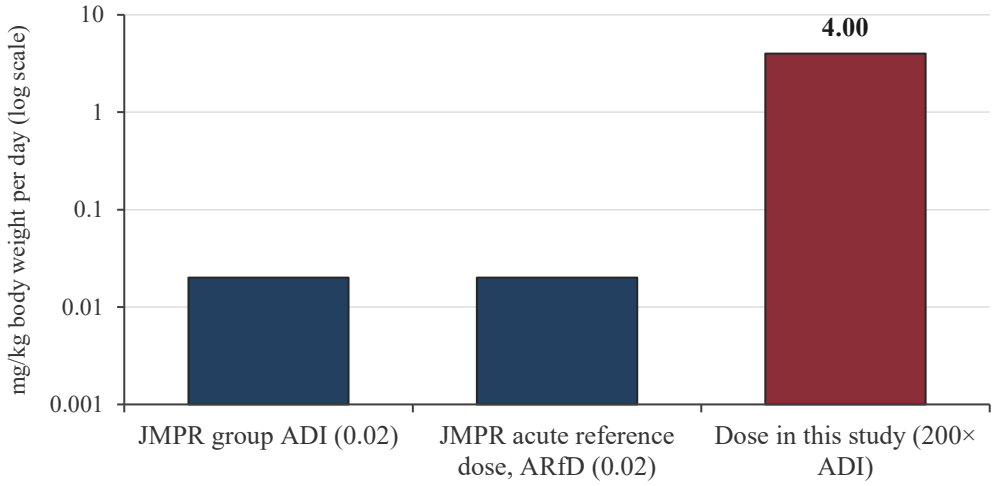
Natural Resources for Human Health
eISSN: 2583-1194

A parallel regional series examined fipronil at 4 mg/kg/day in the same model [1]. The present manuscript addresses the Vantex–control contrast, which corresponds to the histological and immunohistochemical plates presented here; the fipronil arm is used only for mechanistic comparison in the Discussion.

2.3. Experimental design and sampling

Offspring of both groups were removed from the experiment on postnatal days (PND) 7, 14, 21 and 30 by decapitation under light ether anaesthesia [2]. These ages span the transition from mixed to definitive nutrition and the appearance of tertiary follicles — intervals previously identified as critical for ovarian structural reorganisation [1,15]. Thirty dams were allocated to each group [2], and offspring were drawn from the litters of both groups at each of the four ages. The exact number of pups examined per group per age and the number of contributing litters were not recorded in the primary protocol; the consequences of this are set out in Section 4.7. Sampling was standardised to the left ovary and the mid-portion of the uterine horn, with the uterine bifurcation examined separately.

A Administered dose against JMPR reference values



B Mother–offspring protocol

	Gestation	Lactation and postnatal sampling period			
		PND 7	**PND 14**	**PND 21**	**PND 30**
Group 2: Vantex, 4.0 mg/kg/day, oral	Daily maternal exposure, without interruption				
Group 1: intact controls	No exposure				
Offspring sampling		•	•	•	•
Dams per group	n = 30				

Figure 1. Dose context and experimental design. (A) The daily maternal dose used in this study (4.0 mg/kg body weight) shown on a logarithmic scale against the Joint FAO/WHO Meeting on Pesticide Residues group acceptable daily intake and acute reference dose for cyhalothrin and lambda-cyhalothrin (0.02 mg/kg body weight) [22]; the dose exceeds the group acceptable daily intake by approximately 200-fold and is therefore a deliberate experimental challenge rather than a model of dietary intake. (B) Timeline of the mother–offspring protocol, showing continuous maternal exposure through gestation and lactation and the four postnatal sampling points. n = 30 dams per group [2].

2.4. Uterine angioarchitecture

For reconstruction of the uterine vascular bed, Gerota mass was infused slowly through the abdominal aorta; specimens were then cleared according to the method of T.A. Sagatov and processed to paraffin [2,16]. Cleared preparations were used to assess the course, branching order, calibre and distribution density of intramural arteries, veins and postcapillary venules, and to identify avascular territories and blindly ending capillaries.

2.5. Light microscopy

Tissue fragments 0.3–0.6 mm in thickness taken from representative regions of the uterus and ovary were fixed in Carnoy fluid or in 10% neutral buffered formalin, dehydrated through graded alcohols and embedded in paraffin. Sections 5–7 μm thick were stained with haematoxylin and eosin and by the van Gieson method for connective tissue [2]. Photomicrographs were recorded with a transmitted-light microscope fitted with a digital camera at total magnifications of ×100, ×200 and ×400 (ocular ×10 combined with objectives ×10, ×20 and ×40).

2.6. Immunohistochemistry

Proliferating cells were labelled with a rabbit monoclonal antibody against Ki-67 (clone 30-9, Ventana Medical Systems, Roche Diagnostics) [2]. The anti-apoptotic protein Bcl-2 was detected with a rabbit monoclonal anti-Bcl-2 antibody supplied for the same automated platform (Ventana Medical Systems, Roche Diagnostics). Automated staining was performed on the Ventana BenchMark XT platform (Roche Diagnostics, Switzerland) with 3,3′-diaminobenzidine (DAB) chromogen, following the manufacturer's standard protocols. Sections were counterstained with methylene blue and neutral red [2]. Positive signal was read as dark-brown staining of the nucleus and nucleolus for Ki-67 and as brown cellular staining for Bcl-2, in each case against the counterstain. Staining was performed in runs that included the platform manufacturer's standard on-slide controls; dedicated negative controls with the primary antibody omitted and separate positive control tissues are not documented for this series, and this is stated among the limitations (Section 4.7).

2.7. Evaluation of sections

The analytical endpoint of this study is qualitative and semi-quantitative pathomorphology. The following features were assessed systematically in each specimen: vessel calibre and course; presence of congestion, spasm or avascular zones; stromal collagen and elastic fibre density; follicular staging; atresia; thecal and luteal integrity; and the topography and intensity of Ki-67 and Bcl-2 labelling. At least ten non-adjacent sections per organ were reviewed. Sections were assessed by the author. Formal blinding of the observer to treatment group was not applied, and this is reported among the limitations (Section 4.7).

2.8. Data handling and statistical considerations

No inferential statistical testing was performed, and no absolute stereological counts — fractionator follicle numbers or vessel profiles per square millimetre with full unbiased sampling — were generated for the present study. Ratios quoted in the text, in particular the approximately 1.3-fold widening of medullary venule lumen at PND 21 and the approximately 1.7-fold physiological increase of uterine venous profiles by late postnatal life in controls, are the directional values reported in the precursor publications of the same experimental series [1,2] and are cited as such. They are not re-derived measurements of the present material and must not be read as effect-size estimates. The consequences of this design choice are set out in Section 4.7.

2.9. Ethical approval

All procedures involving animals complied with the institutional regulations of Tashkent State Medical University and with the principles of the European Convention for the Protection of Vertebrate Animals used for Experimental and Other Scientific Purposes (ETS No. 123). The protocol was approved by the Ethics Committee of Tashkent Medical Academy. Reporting follows the ARRIVE 2.0 essential-10 items as far as the retrospective nature of the morphological series allows.

3. RESULTS

3.1. Postnatal development of the uterine vascular bed in control offspring

On PND 7–14, sections through the uterine bifurcation of control pups showed incomplete differentiation of the mural layers. The prospective endometrium was still a narrow cellular band without coiled glands, and the myometrium was only beginning to separate into outer longitudinal and inner circular sheets. Intra-organ vessels predominated in the myometrial interstitium between the two muscle systems, while smaller vessels were distributed evenly in the mucosa. Vascular complexes in the

intermuscular space typically contained one or two arteries accompanied by two or three thin-walled veins. Endothelial nuclei were plump and hyperchromatic relative to smooth-muscle nuclei, and the adventitia merged into the surrounding loose connective tissue without a sharp boundary. Towards the cervical portion, vascular bundles formed a hilum containing large cavernous veins of irregular contour with tortuous thin walls [2].

By approximately PND 15 the mucosa and the inner myometrial layer had thickened and become richer in arterial and venous profiles. In the bifurcation zone the characteristic pairing in intermuscular spaces approached one artery with two veins, or two arteries with four veins. Venous walls acquired an inner endothelial lining with two rows of circularly arranged myocytes, whereas postcapillary venules of the outer muscle layer remained lined only by endothelium and fibrous elements without a complete media; these venules were often spatially segregated from arteries. Towards the apex of the uterine horn the absolute number of venous calibres decreased, and first-order veins remained fewer than at the bifurcation.

By PND 30 the total venous population had nearly doubled relative to early postnatal values. Orderly veins were concentrated in the outer and inner myometrium, and postcapillary venules were enriched in the middle and upper segments, corresponding to an approximately 1.7-fold increase across calibres as reported for this model [2]. Clearing preparations after Gerota infusion indicate that this enrichment is not a random hyperaemia but an organised expansion of exchange surface synchronised with myometrial growth. These topographic rules, established in intact animals, provide the baseline against which exposure-induced rarefaction and congestion must be judged, and they agree with the general pattern of age-related change described for organs of the female reproductive system [24].

3.2. Uterine vascular and tissue changes after maternal Vantex exposure

At PND 7 the earliest deviation in exposed offspring was microvascular. Capillaries of the mucosa and outer myometrium were dilated and engorged, the stroma was oedematous, and sparse mononuclear cells appeared between muscle bundles. Epithelial injury was still modest at this age, indicating that vascular dysregulation precedes overt parenchymal destruction.

At PND 14 control uteri showed clear thickening of the mucosa, enrichment of intramural vessels and the appearance of glandular buds. Exposed offspring instead retained mucosal hyperaemia and displayed foci of microhaemorrhage. Spastically narrowed arterioles coexisted with dilated postcapillary venules — an unstable haemodynamic pattern. Endothelial swelling was exaggerated, sludging was evident, and blindly ending capillaries were found in atrophic mucosa, leaving endometrial glands in an architectural dead-end.

Between PND 21 and PND 30 the divergence became structural. Control animals completed the substantial expansion of the venous bed described above, whereas exposed offspring never achieved that trajectory: spastically narrowed vessels increased in number, avascular territories expanded, fibrous septa thickened, and regenerative foci remained small and slow. Microaneurysmatic venous remodelling pointed to intramural congestion. The morphological message is that, without a competent hemomicrocirculatory scaffold, mural differentiation of the juvenile uterus is arrested at a reactive, fibrotic stage.

3.3. Ovarian morphology after maternal Vantex exposure

Control ovaries at PND 7 contained nests of oocytes partially enclosed by flattened pre-granulosa cells, with loose, richly capillarised medullary mesenchyme. By PND 14 corticomedullary demarcation was clear, primary follicles were frequent, and secondary follicles with two or more granulosa layers appeared near the hilum. The nuclear–cytoplasmic (N/C) ratio of follicular epithelium remained low, and atresia occurred at a low baseline rate commensurate with physiological selection of the follicular pool. Collagen and elastic fibres of the cortex formed a fine mesh with delicate borders between connective septa.

PND 14. Ovaries of exposed offspring already differed from age-matched controls. Packing density of collagen and elastic fibres in the stroma was increased, particularly in meshworks abutting follicles and central medullary vessels, and elastic fibres became irregularly condensed beneath the tunica albuginea. Inflammatory-destructive remodelling of vascular–tissue units coexisted with acceleration of folliculogenesis [1]. Cortical and medullary compartments remained recognisable. Primary follicles were present together with immature primordial follicles whose epithelial nuclei were enlarged and relatively hyperchromatic compared with the physiological pattern, and the surface mesothelium formed an uneven contour (Figure 2). Capillaries and venules trapped within the densified septa displayed uneven contours, an early morphological correlate of the avascular zones seen later.

Natural Resources for Human Health
eISSN: 2583-1194

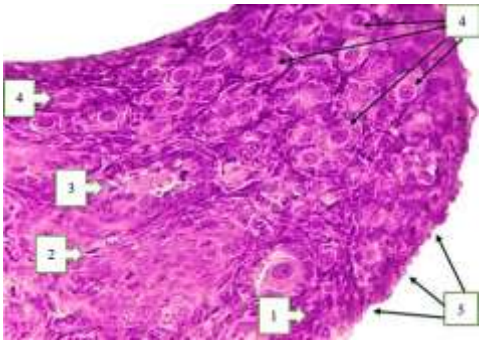


Figure 2. Ovary of a postnatal day 14 offspring from a Vantex-exposed dam. Cortex (1); medulla (2); primary follicles (3); immature primordial follicles with enlarged, relatively hyperchromatic epithelial nuclei (4); uneven surface mesothelium (5). Haematoxylin and eosin; objective ×20 (total magnification ×200).

PND 21. Distortion of the N/C ratio in the epithelium of immature primordial follicles became more evident. Under physiological conditions this ratio is low, the nucleus being small while the cytoplasm occupies a wider area; in exposed offspring the reverse pattern prevailed. Oocytes located in the centre of follicles underwent atresia before completing maturation. Interstitial tissue contained proliferative foci. Theca cells followed heterogeneous trajectories, became oval and showed dystrophic and necrotic change (Figure 3) [1]. These nuclear changes are not trivial cytological curiosities: they imply altered chromatin packing in cells that must later support oocyte growth.

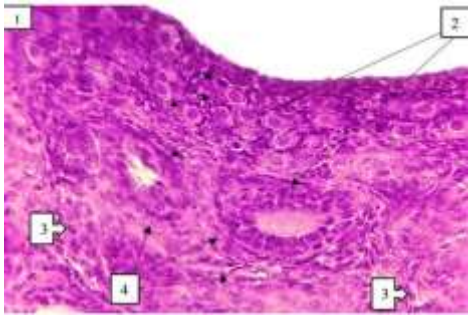


Figure 3. Ovary, postnatal day 21, Vantex group. Enlarged epithelial nuclei with altered nuclear–cytoplasmic index (1); atresia of the centrally placed oocyte (2); interstitial proliferative foci (3); dystrophic and necrotic theca cells (4). Haematoxylin and eosin; objective ×40 (total magnification ×400).

PND 30. Injury extended into luteal tissue. Corpora lutea contained multiple necrotic foci among luteocytes, while adjacent interstitial cells retained proliferative clusters (Figure 4). The lesion was therefore not confined to the pre-ovulatory follicular pool but compromised the endocrine support expected after the first juvenile cycles. The interstitial proliferative foci visible at PND 21–30 should not be mistaken for healthy repair: their topography is patchy, their cytological composition mixed, and they coexist with necrotic theca and luteocytes.

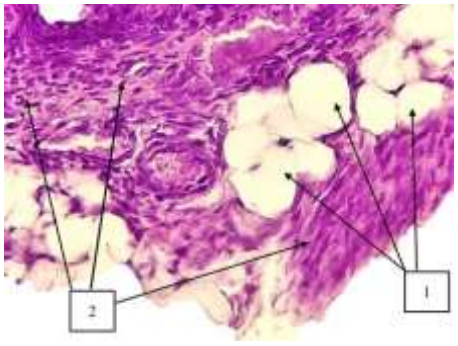


Figure 4. Ovary, postnatal day 30, Vantex group. Necrotic foci among luteocytes of the corpus luteum (1); proliferative foci in adjacent interstitial cells (2). Haematoxylin and eosin; objective ×40 (total magnification ×400).

3.4. Hemomicrocirculatory remodelling

The ovarian vascular bed comprises arterioles, capillaries and venules. Under Vantex exposure, luminal widening persisted at PND 21 while mural thickness decreased relative to controls; medullary venule lumen was approximately 1.3-fold larger than in intact animals [1]. Early after intoxication (PND 7–14) both uterus and ovary exhibited marked hyperaemia, microvessel dilatation, stromal oedema and mononuclear infiltration, with occasional mucosal microhaemorrhages [2]. In later windows (PND 21–30) the pathomorphological vascular–tissue alterations progressed: spastically narrowed vessels increased, avascular territories expanded, and fibrosis replaced regenerative attempts that remained weak and slow.

In the comparative fipronil arm, thinning of all vascular coats, intensified fibrosis, connective-tissue overgrowth and avascular zones with blindly ending capillaries were conspicuous, especially in regions of trophic failure [1]. These observations indicate that microvascular rarefaction is a shared downstream pathway of chemically dissimilar insecticides even though their primary molecular targets differ.

Across PND 14–21 — the window of transition to definitive nutrition, during which tertiary follicles begin to form in intact rats — exposed offspring showed hyperchromasia of follicular epithelial nuclei, nutrient deficiency around the oocyte and haemorrhagic inclusions [1]. Persistence of these signs into later postnatal life indicates incomplete compensation, consistent with toxic persistence of residual pyrethroid stored in the adipose tissue of the pup [2].

3.5. Ki-67 and Bcl-2 immunoreactivity

Because most cortical ovarian cells belong to the reproductive-cycle compartment, proliferative and anti-apoptotic markers were assessed alongside the structural analysis. In the uterus of exposed offspring at PND 14, Ki-67 positivity was concentrated in the isthmicocervical glandular epithelium, with only scattered positive stromal cells (Figure 5). This topography indicates reactive epithelial turnover in a mucosa whose vascular support is already compromised, and suggests that the cervical end of the Müllerian duct derivatives is particularly reactive under toxic stress.

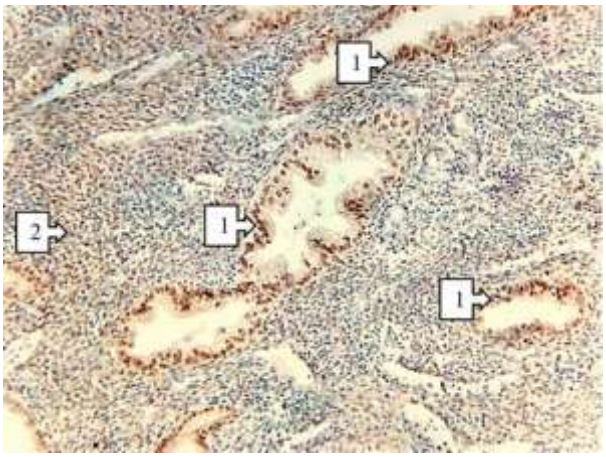


Figure 5. Uterus, postnatal day 14, Vantex group. Ki-67-positive glandular epithelial cells in the isthmicocervical region (1) and scattered positive stromal cells (2). Immunohistochemistry, DAB chromogen with haematoxylin counterstain; objective ×10 (total magnification ×100).

In the ovary at PND 21, Ki-67 labelled both parenchymal and stromal compartments (Figure 6). Dark-brown nuclear staining was interpreted as compensatory replenishment of cells lost to apoptosis and atresia; the rapid rise of stromal Ki-67 under exposure is consistent with that reading [2].

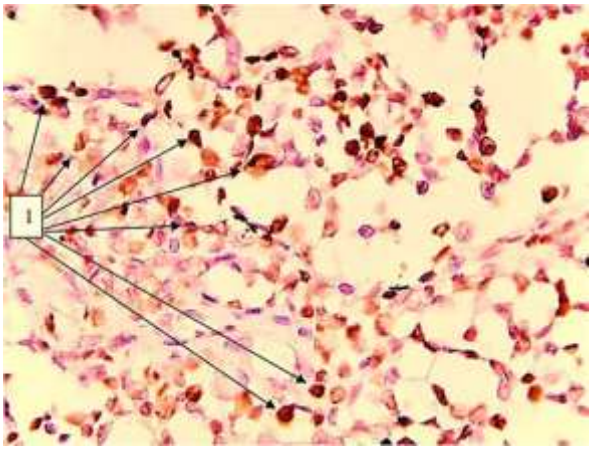


Figure 6. Ovary, postnatal day 21, Vantex group. Ki-67-positive parenchymal and stromal cells (1). Immunohistochemistry, DAB chromogen with haematoxylin counterstain; objective ×20 (total magnification ×200).

By PND 30, Bcl-2 immunoreactivity remained clearly detectable in ovarian tissue (Figure 7). Persistent anti-apoptotic signalling alongside ongoing necrosis and atresia suggests an incomplete compensatory response in which cells resist death while the microvascular niche remains inadequate for orderly repair. The combination of elevated Ki-67 and persistent Bcl-2 is not self-contradictory: Bcl-2 may protect a subset of cells from immediate execution while Ki-67 marks neighbours recruited into the cycle.

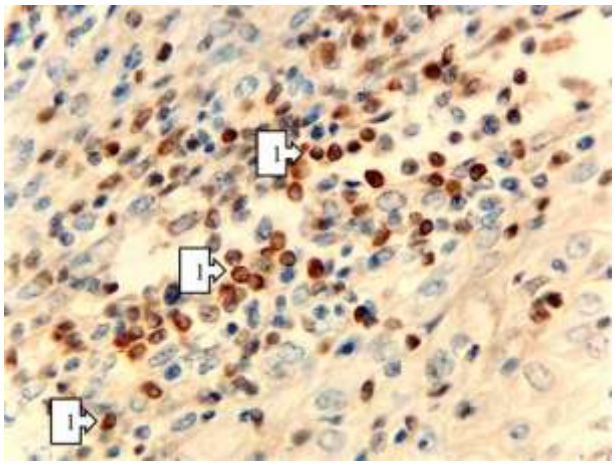


Figure 7. Ovary, postnatal day 30, Vantex group. Bcl-2-positive expression (1). Immunohistochemistry, DAB chromogen with haematoxylin counterstain; objective ×40 (total magnification ×400).

3.6. Summary of group differences

The principal morphological contrasts between control and exposed offspring are collected in Table 1.

Table 1. Comparative morphological profile of control and Vantex-exposed offspring. Entries summarise qualitative observations of the present series together with directional findings reported for the same experimental model in [1,2].

Feature	**Control offspring**	**Vantex-exposed offspring**
Ovarian stroma (PND 14–21)	Balanced fibre density; orderly follicles	Collagen and elastic fibre condensation; inflammatory-destructive foci
Primordial follicular epithelium	Small nuclei, wide cytoplasm; low N/C index	Enlarged hyperchromatic nuclei; altered N/C index

Natural Resources for Human Health
eISSN: 2583-1194

Oocyte fate	Progressive maturation; baseline atresia	Premature atresia of centrally placed oocytes
Theca and luteal tissue	Preserved architecture	Dystrophy and necrosis; necrotic foci among luteocytes by PND 30
Medullary venules (PND 21)	Baseline calibre	Lumen ≈ 1.3× control; thinner wall [1]
Uterine venous bed (to PND 30)	≈ 1.7–2× enrichment vs early PND [2]	Expansion blunted; spasm, avascular zones, fibrosis
Ki-67	Age-appropriate low to moderate labelling	Increased in isthmicocervical glands, ovarian parenchyma and stroma
Bcl-2 (PND 30)	Low	Clearly positive

N/C, nuclear–cytoplasmic; PND, postnatal day. Ratios marked with a reference are directional values reported in the cited precursor publications and were not re-measured in the present material (Section 2.8).

3.7. Quantitative statements and semi-quantitative severity profile

The precursor publications of this experimental series report three numeric values; these are reproduced in Figure 8 together with their sources. At PND 21 the lumen of ovarian medullary venules in exposed offspring was approximately 1.3 times that of intact animals [1] (Figure 8A). In control animals the uterine venous bed expanded approximately 1.7-fold across all calibres, and the total count of venous vessels approximately doubled, between early postnatal life and PND 30 [2] (Figure 8B). That physiological expansion was blunted in exposed offspring, although the source does not quantify the shortfall. No further numeric data were generated in the series, and Section 2.8 explains why none are re-derived here.

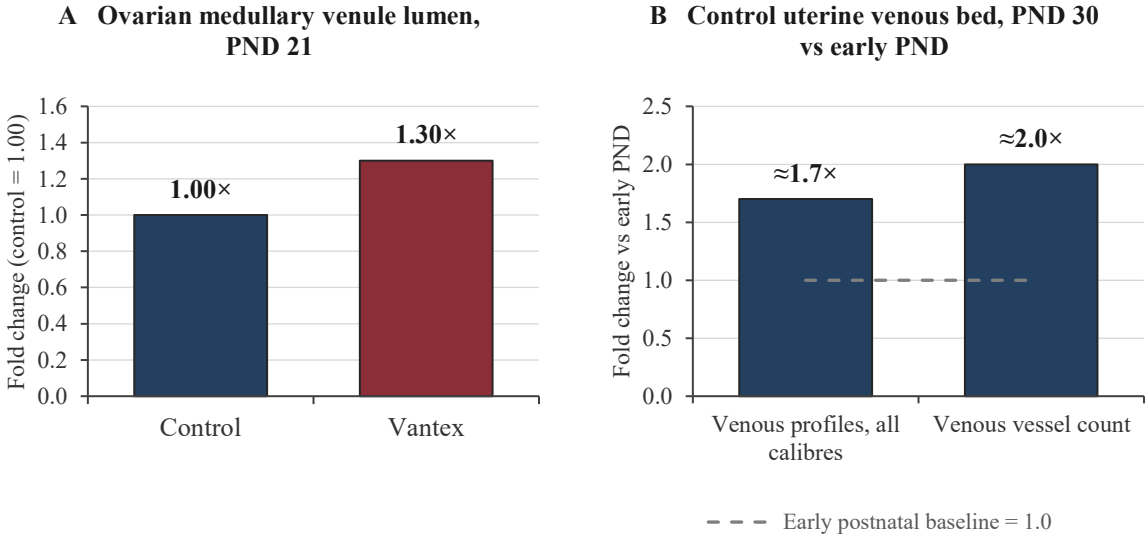


Figure 8. Quantitative statements reported for this experimental model. (A) Ovarian medullary venule lumen at postnatal day 21, expressed as fold change relative to intact controls [1]. (B) Physiological expansion of the uterine venous bed in control offspring at postnatal day 30 relative to early postnatal life [2]; this expansion is blunted after maternal exposure, but the source does not quantify the shortfall. Panels A and B answer different questions and must not be read as a single comparison. No value in this figure was measured for the present article.

To give the descriptive findings a reproducible structure, each morphological feature was scored semi-quantitatively on a four-point ordinal scale (0 = absent, 1 = mild, 2 = moderate, 3 = marked) at each sampling age. The resulting profile is set out in Table 2 and displayed in Figure 9. The scoring isolates a pattern that the narrative description implies but does not separate:

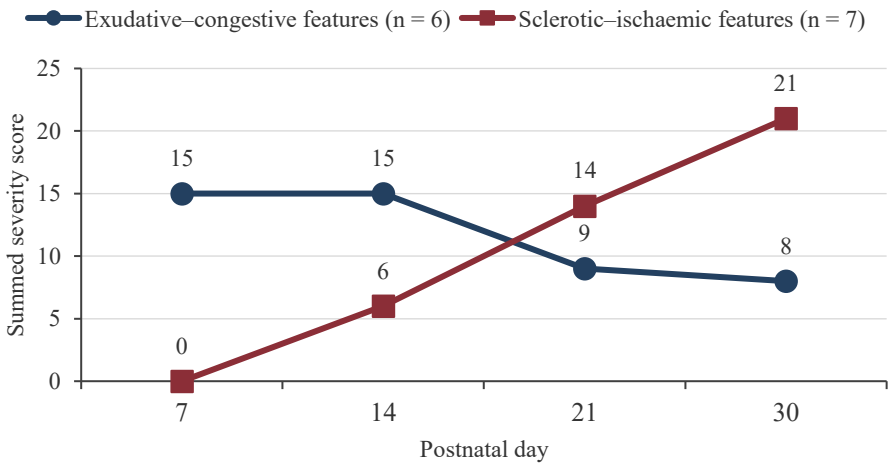
exudative–congestive features — hyperaemia, microvessel dilatation, stromal oedema, mononuclear infiltration, mucosal microerosion and intracapillary sludge — peak at PND 7–14 and then decline, whereas sclerotic–ischaemic features — spastic narrowing, avascular zones, fibrosis and thinning of the vascular coats — together with follicular and luteal injury rise steadily to PND 30 (Figure 9A). The two trajectories cross between PND 14 and PND 21, the same window in which tertiary follicles normally appear. The lesion therefore does not simply intensify with time; it changes character, from a potentially reversible exudative reaction to an established sclerotic–ischaemic state.

Table 2. Semi-quantitative severity profile of morphological features in the Vantex group across postnatal days. 0 = absent, 1 = mild, 2 = moderate, 3 = marked.

Morphological feature	PND 7	PND 14	PND 21	PND 30
Hyperaemia / venous congestion	3	3	2	2
Microvessel dilatation	3	3	2	1
Stromal oedema	3	2	1	1
Mononuclear / leukocyte infiltration	2	3	2	2
Mucosal microerosion / haemorrhage	2	2	1	1
Sludge / microthrombi in capillaries	2	2	1	1
Spastically narrowed vessels	0	1	2	3
Avascular zones / blind-ending capillaries	0	1	2	3
Fibrosis / connective-tissue overgrowth	0	1	2	3
Thinning of vascular coats	0	1	2	3
Stromal fibre condensation (ovary)	1	2	2	2
Premature oocyte atresia	0	1	3	3
Thecal dystrophy / necrosis	0	1	2	3
Luteocyte necrosis	0	0	1	3
Ki-67 labelling above age-matched control	1	2	3	2
Bcl-2 labelling above age-matched control	0	1	2	3
Total (16 features)	**17**	**26**	**30**	**36**

PND, postnatal day. Scores were assigned by the author from the morphological descriptions and plates of this experimental series; they are an ordinal summary, not a measurement, and were not tested statistically. The wording of the source text underlying each score is given in the accompanying data workbook.

A Shift in the character of the lesion



B Semi-quantitative severity profile

	PND 7	PND 14	PND 21	PND 30
Hyperaemia / congestion	3	3	2	2
Microvessel dilatation	3	3	2	1
Stromal oedema	3	2	1	1
Mononuclear infiltration	2	3	2	2
Microerosion / haemorrhage	2	2	1	1
Sludge / microthrombi	2	2	1	1
Spastic narrowing	0	1	2	3
Avascular zones	0	1	2	3
Fibrosis	0	1	2	3
Thinning of coats	0	1	2	3
Oocyte atresia	0	1	3	3
Thecal dystrophy	0	1	2	3
Luteocyte necrosis	0	0	1	3
Score scale	0 absent	1 mild	2 moderate	3 marked

Figure 9. Semi-quantitative severity profile of the Vantex group. (A) Summed scores for six exudative–congestive features and for seven sclerotic–ischaemic and parenchymal features across postnatal days 7–30; the trajectories cross between postnatal days 14 and 21. (B) The underlying score matrix (0 = absent, 1 = mild, 2 = moderate, 3 = marked); the rule separates the two feature groups. Scores are an ordinal summary of the qualitative observations assigned by the author, not measurements, and were not tested statistically. The full scoring sheet, with the wording of the source text on which each score rests, is provided in the accompanying data workbook. Scores were assigned by the author from the morphological descriptions and plates of the present series. They constitute an ordinal summary of qualitative observations, not a measurement, and no statistical comparison was performed on them. They are reported so that a reader can see which features drove the interpretation and can disagree with any individual score.

3.8. Proposed sequence of events

The observations above are internally consistent and can be arranged as a single sequence running from maternal exposure through microvascular failure to follicular and luteal injury and finally to an unsuccessful compensatory response (Figure 10). Figure 10 is a concept diagram summarising the interpretation offered in this article; it is not derived from measured data and carries no quantitative claim.

	Maternal chronic exposure Vantex (gamma-cyhalothrin), 4.0 mg/kg/day by mouth, continued through gestation and lactation
	↓
PND 7 vascular change precedes parenchymal damage	**Transfer to offspring** Transplacental passage and lactational transfer; retention in lipid-rich compartments of the pup
	↓
	Primary cellular hit Pyrethroid action on excitable membranes and lipid bilayers; oxidative amplification (MDA ↑, SOD / CAT / GSH ↓) → endothelial and follicular epithelial injury
	↓

PND 14 stromal condensation, nuclear hyperchromasia	**Hemomicrocirculatory failure** Dilatation and congestion (PND 7–14) → spasm, rarefaction and avascular zones (PND 21–30); blunted physiological expansion of the uterine venous bed
	↓
	Trophic deficit in the developing gonad Reduced delivery of oxygen and substrates to growing follicles and to the maturing myometrium
	↓
PND 21 medullary venule lumen ≈ 1.3× control	**Tissue injury** Altered nuclear–cytoplasmic index of primordial epithelium; premature central oocyte atresia; thecal dystrophy; necrotic foci in luteocytes; stromal fibre condensation
	↓
PND 30 luteocyte necrosis; Bcl-2 still positive	**Compensatory response — incomplete** Ki-67 ↑ in glandular epithelium, parenchyma and stroma; Bcl-2 persistently positive at PND 30 — proliferation without perfusion yields disordered cellularity

Figure 10. Proposed pathogenetic sequence linking chronic maternal Vantex exposure to disturbed postnatal utero-ovarian morphogenesis. This is a schematic concept diagram summarising the interpretation presented in Sections 3 and 4; it is not derived from measured data and expresses no quantitative claim. The ratio shown for postnatal day 21 is the directional value reported in [1].

4. DISCUSSION

4.1. Principal findings

The morphological series presented here supports a coherent pathogenetic sequence in which chronic low-dose maternal exposure to Vantex destabilises the postnatal establishment of utero-ovarian vascular–tissue modules. Three features deserve emphasis. First, the earliest detectable change is vascular rather than parenchymal, appearing at PND 7 when epithelial injury is still modest. Second, the physiological expansion of the uterine venous bed that normally accompanies myometrial growth is blunted, so the deficit is developmental rather than a transient haemodynamic fluctuation. Third, proliferative and anti-apoptotic markers rise in a pattern that signals attempted repair without architectural restoration.

4.2. Mechanistic interpretation

Three interlocking mechanisms plausibly link exposure to the observed morphology. Pyrethroid action on excitable membranes and lipid bilayers provides a primary hit on endothelium and follicular epithelium consistent with the known interaction of type II pyrethroids with voltage-gated sodium channels and membrane lipids [5,17]. Oxidative amplification converts sublethal membrane stress into mitochondrial dysfunction and cell death: Ghosh and colleagues showed that short-term oral exposure to lambda-cyhalothrin elevates ovarian malondialdehyde, depletes glutathione-dependent antioxidant enzymes and disrupts the oestrous cycle [10], and that the lesion extends to hepatic and lipid-metabolic biomarkers with partial rescue by taurine [11]. Finally, chronic hypoperfusion secondary to rarefaction, spasm and venous congestion locks the gonad into a high-turnover, low-function state in which proliferation does not rebuild a normal follicular hierarchy. The necrotic luteal foci and atretic oocytes reported here are morphological counterparts of that biochemical lesion, observed not after direct dosing of juvenile females but after maternal transfer — an epidemiologically more relevant route.

Endocrine disruption adds a further layer. Lambda-cyhalothrin reduces ovarian 3β- and 17β-hydroxysteroid dehydrogenase activity and steroidogenic acute regulatory protein expression and lowers oestradiol and progesterone [12], and comparative work across vertebrates identifies several molecular routes by which pyrethroids act as endocrine disruptors [19]. The parent compound also induces hepatic cytochrome P450 enzymes, oxidative stress and apoptosis, which bears on systemic handling of the toxicant in the dam and the pup [21]. Although steroid assays were not repeated in the present morphological study, the necrotic luteal phenotype is what one would expect when steroidogenic machinery fails inside an ischaemic corpus luteum. The

mononuclear infiltration observed at early time points is also consistent with the immunotoxic properties attributed to pesticide exposure more generally [23].

4.3. Microcirculation as the organising endpoint

Many reproductive toxicology studies report organ weight, hormone concentrations or fertility indices without reconstructing the vessels that deliver substrates to follicles and myometrium. Classical morphology has long held that the ovary is a highly vascular organ whose follicular selection is inseparable from thecal capillarisation, and that the uterus undergoes staged enrichment of intramural veins during postnatal growth [2,15,16]. If a toxicant thins vascular coats, reduces anastomoses and creates avascular territories, every downstream endocrine measurement will be secondarily abnormal; measuring hormones alone therefore risks mistaking consequence for cause. The present design inverts that hierarchy, beginning with vessels and tissue structure and using Ki-67 and Bcl-2 only as cellular commentaries on the structural lesion.

Reviews of pesticide effects on the ovary emphasise that pyrethroids can reduce follicle and corpus luteum numbers, elevate atresia and disturb gonadotropin and sex-steroid profiles even at comparatively low doses [9,18]. The present data add the vascular dimension that is usually under-reported: when anastomoses decrease, venous congestion rises and avascular territories expand, Ki-67-positive regeneration becomes reactive rather than constructive, and Bcl-2 upregulation fails to restore a normal follicular hierarchy.

4.4. Comparison with fipronil and with other pyrethroids

Comparison with fipronil is instructive. Phenylpyrazoles antagonise GABA-gated chloride channels and can delay vaginal opening and alter cyclicity without always producing gross ovarian histological change at low perinatal doses [13,14]. In the regional fipronil arm of the same experimental programme, however, fibrotic encapsulation and avascular scarring were evident [1]. Dose, timing and morphological resolution therefore jointly determine whether reproductive toxicity is classified as functional only or as structural–functional, and dual-class agricultural exposure, common in field practice, may produce additive harm precisely at the microvascular level.

Fenvalerate, cypermethrin and permethrin have all been shown to reduce preantral follicle and corpus luteum numbers, increase atresia and disturb gonadotropins in rodent offspring or adults [9,18,20]. Against that background, Vantex at 4 mg/kg/day in a maternal chronic model is not an exotic high-dose curiosity but a field-relevant pyrethroid challenge that reproduces the ovarian lesion class while documenting the microvascular mediator in early postnatal life. The study does not claim that Vantex is uniquely toxic among pyrethroids; it shows that a representative modern formulation, applied chronically at a low daily dose to the mother, suffices to derange postnatal utero-ovarian morphogenesis through a microvascular pathway. That claim is narrower, more testable and more useful for prevention than an undifferentiated statement that pesticides are harmful.

4.5. Interpretive caveats for immunohistochemistry

DAB chromogen yields a permanent brown deposit that is well suited to archival plates but requires careful discrimination from haemosiderin and from overlapping nuclei. In the present series Ki-67 was read only as crisp nuclear signal and Bcl-2 as cytoplasmic and membrane-compatible cellular signal matching antibody expectations. Elevated Ki-67 does not by itself equal healthy proliferation: in oncology the marker indicates growth fraction, whereas in developmental toxicology it may indicate either a repair attempt or dysregulated cycling. Only the combination with architecture (Figures 2–4) and with the state of the vascular bed permits the reading offered here, namely compensatory, incomplete and ultimately unsuccessful proliferation. The isthmicocervical predominance of uterine Ki-67 at PND 14 warrants dedicated quantification in a follow-up stereological study.

4.6. Translational and regulatory implications

From a developmental standpoint, protecting microvascular maturation during late fetal and early postnatal life may be as important as protecting germ cells when perinatal interventions are designed [15]. Women of fertile age in agrarian regions may accumulate pyrethroid residues through occupational spraying, household use and diet [4,5]. Counselling should include minimisation of pyrethroid use during preconception and lactation, preference for non-chemical indoor pest control, and early evaluation of menstrual irregularities in adolescents with documented household exposure. Experimental morphology of the kind presented here supplies biological plausibility for epidemiological associations between pyrethroid metabolites and reproductive endpoints [8,9,18].

Regulatory toxicology traditionally emphasises no-observed-adverse-effect levels derived from adult multigeneration assays, and international residue evaluations of cyhalothrin compounds are framed in those terms [22]. The postnatal vascular–tissue endpoints described here suggest that juvenile morphological batteries — angioarchitecture, follicle staging and Ki-67/Bcl-2 topography — would increase sensitivity for detecting developmental reproductive toxicity of modern pyrethroids and deserve consideration in national registration dossiers. Values derived only from adult fertility indices may miss the structural injury documented here at PND 14–30.

4.7. Strengths and limitations

The principal strength of the design is exposure realism. Direct gavage of adult females with high fractions of the median lethal dose demonstrates hazard but not the perinatal route that matters for public health, whereas maternal chronic low-dose exposure with transfer across placenta and milk reproduces the pathway by which agrarian communities contaminate the next generation [7,13]. The combination of Gerota angioarchitecture, conventional histology and automated immunohistochemistry addresses vessels and parenchyma within the same specimens.

The limitations are substantial and must be stated plainly. No inferential statistics were applied and no unbiased stereological counts were generated, so the study supports directional and qualitative conclusions only; the ratios quoted in Sections 3.1, 3.3 and 3.4 are values reported in the precursor publications of the same series [1,2] rather than measurements of the present material. Litter effects were not modelled with mixed-effects statistics, and because pups from the same dam are not statistically independent this is a material constraint on any future quantitative claim. Serum hormone and oxidative-stress panels were not run in these animals, so the mechanistic account in Section 4.2 is inferential and rests on published work in related compounds. The observer was not blinded to treatment group, dedicated immunohistochemical controls are not documented, and the per-age sample size and the identity of the commercial formulation were not recorded in the primary protocol. Because the administered dose exceeds the JMPR group acceptable daily intake by roughly two orders of magnitude [22], the study establishes a hazard and a mechanism rather than a risk at dietary exposure levels. Scale bars are absent from the original photomicrographs and magnification is reported as the objective–ocular combination. Finally, extrapolation from rat postnatal days to human developmental windows is conceptual rather than quantitative.

4.8. Future directions

A definitive quantitative study should add unbiased stereology — the optical fractionator for follicle numbers and space-ball or length-density probes for vessels — together with litter-based mixed-effects statistics and paired biochemical assays of hormones and redox status in the same animals. Calibrated scale bars should be recorded at acquisition. Such upgrades would not reverse the present qualitative conclusion; they would sharpen effect-size estimates and allow the vascular endpoint to be compared across compounds and laboratories. For morphologists repeating the protocol we recommend a verified delivered dose of 4.0 mg/kg with rotation of application sites, standardised sampling of the left ovary and mid-horn uterus, at least ten non-adjacent sections per organ, dual blinded reading of Ki-67, and archiving of raw images alongside any future stereological tables.

5. CONCLUSIONS

1. Chronic maternal intoxication with Vantex is accompanied by pronounced disturbance of the hemomicrocirculatory bed in the uterus and ovary of offspring: uneven luminal dilatation, tortuosity, reduced distribution density, venous congestion and avascular zones, together with destructive mural change and atrophy of tissue elements.

2. The same exposure disrupts postnatal folliculogenesis, producing hyperchromasia and an altered nuclear–cytoplasmic index of primordial epithelium, premature atresia of centrally placed oocytes, thecal dystrophy and necrotic foci among luteocytes.

3. Increased Ki-67 labelling and persistent Bcl-2 immunoreactivity reflect compensatory proliferative and anti-apoptotic responses that remain insufficient while perfusion is impaired.

4. Microvascular change is detectable before overt parenchymal destruction, and the degree of tissue injury corresponds to the state of the microcirculatory vessels. On these morphological criteria Vantex behaves as a reproductive toxicant in the mother–offspring rat model.

5. Juvenile morphological endpoints that include angioarchitecture merit consideration in the evaluation of modern pyrethroids, and preventive measures are warranted for women of reproductive age with chronic pyrethroid contact.

REFERENCES

[1] Khozhanazarova SZh. The effect of pesticides on the state of the microvasculature and tissue structures of the ovaries in rats. Vestnik of Tashkent Medical Academy. 2023;(9):54–58.

[2] Khozhanazarova SZh, Gulmanov ID, Yusupova MA, Ziyoeva GP, Razhabov BM, Egamberdieva LY. Morphological state of the microcirculation bed and tissue structures of the uterine and ovarian in chronic intoxication with pesticide. Tibbiyotda yangi kun (New Day in Medicine). 2023;1(51):49–55. ISSN 2181-712X; EISSN 2181-2187.

[3] Anudina AV. Toxic effects of pesticides on the human and animal organism. International Student Scientific Herald. 2019;(1):22–25.

[4] Tang W, Wang D, Wang J, Wu Z, Li L, Huang M, Xu S, Yan D. Pyrethroid pesticide residues in the global environment: an overview. Chemosphere. 2018;191:990–1007. doi:10.1016/j.chemosphere.2017.10.115

[5] Saillenfait AM, Ndiaye D, Sabaté JP. Pyrethroids: exposure and health effects — an update. Int J Hyg Environ Health. 2015;218(3):281–292. doi:10.1016/j.ijheh.2015.01.002

[6] Mostafalou S, Abdollahi M. Pesticides and human chronic diseases: evidences, mechanisms, and perspectives. Toxicol Appl Pharmacol. 2013;268(2):157–177. doi:10.1016/j.taap.2013.01.025

[7] Istamova ShA, Utepova NE, Tukhtaev SN. Postnatal development of endocrine and immune organs of offspring under intrauterine pesticide exposure. Tashkent: Tashkent State Medical University Repository; 2021.

[8] Mnif W, Hassine AIH, Bouaziz A, Bartegi A, Thomas O, Roig B. Effect of endocrine disruptor pesticides: a review. Int J Environ Res Public Health. 2011;8(6):2265–2303. doi:10.3390/ijerph8062265

[9] Wang L, Ma X, Liu J. Adverse effects of pesticides on the ovary: evidence from epidemiological and toxicological studies. Environ Health (Washington). 2025;3(6):575–595. doi:10.1021/envhealth.4c00243

[10] Ghosh R, Banerjee B, Das T, Jana K, Choudhury SM. Alteration in estrous cycle, lipid peroxidation and antioxidant status in female rat after exposure to lambda-cyhalothrin and its attenuation by taurine. Int J Bioassays. 2015;4(11):4450–4457. doi:10.21746/ijbio.2015.11.0018

[11] Ghosh R, Das T, Paramanik A, Maiti Choudhury S. Lambda-cyhalothrin elicited dose response toxicity on haematological, hepatic, gonadal and lipid metabolic biomarkers in rat and possible modulatory role of taurine. Toxicol Forensic Med Open J. 2016;1(2):42–51. doi:10.17140/TFMOJ-1-107

[12] Ghosh R, Banerjee B, Das T, Jana K, Choudhury SM. Antigonadal and endocrine-disrupting activities of lambda cyhalothrin in female rats and its attenuation by taurine. Toxicol Ind Health. 2018;34(3):146–157. doi:10.1177/0748233717742291

[13] de Barros AL, Rosa JL, Cavariani MM, Borges CS, Villela e Silva P, Bae JH, Anselmo-Franci JA, Arena AC. In utero and lactational exposure to fipronil in female rats: pregnancy outcomes and sexual development. J Toxicol Environ Health A. 2016;79(6):266–273. doi:10.1080/15287394.2016.1149132

[14] Udo MSB, Sandini TM, Reis TM, Bernardi MM, Spinosa HS. Prenatal exposure to a low fipronil dose disturbs maternal behavior and reflex development in rats. Neurotoxicol Teratol. 2014;45:27–33. doi:10.1016/j.ntt.2014.05.010

[15] Cunha GR, Robboy SJ, Kurita T, Isaacson D, Shen J, Cao M, Baskin LS. Development of the human female reproductive tract. Differentiation. 2018;103:46–65. doi:10.1016/j.diff.2018.09.001

[16] Sagatov TA, Khodzhanazarova SKh, Yusupova NT, Nishanova NK. Morphological state of the microcirculatory bed and tissue structures of the uterus in chronic intoxication with the pesticide Bi-58. Problems of Science. 2019;(8):52–58.

[17] Soderlund DM. Molecular mechanisms of pyrethroid insecticide neurotoxicity: recent advances. Arch Toxicol. 2012;86(2):165–181. doi:10.1007/s00204-011-0726-x

[18] Ye X, Liu J. Effects of pyrethroid insecticides on hypothalamic-pituitary-gonadal axis: a reproductive health perspective. Environ Pollut. 2019;245:590–599. doi:10.1016/j.envpol.2018.11.031

[19] Brander SM, Gabler MK, Fowler NL, Connon RE, Schlenk D. Pyrethroid pesticides as endocrine disruptors: molecular mechanisms in vertebrates with a focus on fishes. Environ Sci Technol. 2016;50(17):8977–8992. doi:10.1021/acs.est.6b02253

[20] Marettova E, Maretta M, Legáth J. Effect of pyrethroids on female genital system. Review. Anim Reprod Sci. 2017;184:132–138. doi:10.1016/j.anireprosci.2017.07.007

[21] Martínez MA, Ares I, Rodríguez JL, Martínez M, Roura-Martínez D, Castellano V, Lopez-Torres B, Martínez-Larrañaga MR, Anadón A. Pyrethroid insecticide lambda-cyhalothrin induces hepatic cytochrome P450 enzymes, oxidative stress and apoptosis in rats. Sci Total Environ. 2018;631–632:1371–1382. doi:10.1016/j.scitotenv.2018.03.030

[22] Food and Agriculture Organization of the United Nations / World Health Organization. Lambda-cyhalothrin (146). In: Pesticide residues in food 2015 — Joint FAO/WHO Meeting on Pesticide Residues: evaluations. Rome: FAO; 2015. Group ADI 0–0.02 mg/kg bw; ARfD 0.02 mg/kg bw. Available from: https://www.fao.org/fileadmin/user_upload/IPM_Pesticide/JMPR/Evaluations/2015/LAMBDA-CYHALOTHRIN__146_.pdf

[23] Gerunova TV, Redkin YuV, Gerunova LK. Immunotoxicity of pesticides: role in pathology of animals and humans. Advances in Modern Biology. 2011;131(5):474–482.

[24] Alexeev YuD, Ivakhina SA, Efimov AA, Raykova KA. Age-related morphological changes in organs of the female reproductive system. Modern Problems of Science and Education. 2016;(4). Available from: https://science-education.ru/ru/article/view?id=24951

[25] Khozhanazarova SZh. The effect of pesticides on the state of the microvasculature and tissue structures of the ovary. Scholar Express: International Journal of Multidisciplinary Research. Available from: https://scholarexpress.net/index.php/index/article/view/1824

Figure legends

Figure 1. Dose context and experimental design. (A) The daily maternal dose used in this study (4.0 mg/kg body weight) shown on a logarithmic scale against the Joint FAO/WHO Meeting on Pesticide Residues group acceptable daily intake and acute reference dose for cyhalothrin and lambda-cyhalothrin (0.02 mg/kg body weight) [22]; the dose exceeds the group acceptable daily intake by approximately 200-fold and is therefore a deliberate experimental challenge rather than a model of dietary intake. (B) Timeline of the mother–offspring protocol, showing continuous maternal exposure through gestation and lactation and the four postnatal sampling points. n = 30 dams per group [2].

Figure 2. Ovary of a postnatal day 14 offspring from a Vantex-exposed dam. Cortex (1); medulla (2); primary follicles (3); immature primordial follicles with enlarged, relatively hyperchromatic epithelial nuclei (4); uneven surface mesothelium (5). Haematoxylin and eosin; objective ×20 (total magnification ×200).

Figure 3. Ovary, postnatal day 21, Vantex group. Enlarged epithelial nuclei with altered nuclear–cytoplasmic index (1); atresia of the centrally placed oocyte (2); interstitial proliferative foci (3); dystrophic and necrotic theca cells (4). Haematoxylin and eosin; objective ×40 (total magnification ×400).

Figure 4. Ovary, postnatal day 30, Vantex group. Necrotic foci among luteocytes of the corpus luteum (1); proliferative foci in adjacent interstitial cells (2). Haematoxylin and eosin; objective ×40 (total magnification ×400).

Figure 5. Uterus, postnatal day 14, Vantex group. Ki-67-positive glandular epithelial cells in the isthmicocervical region (1) and scattered positive stromal cells (2). Immunohistochemistry, DAB chromogen with haematoxylin counterstain; objective ×10 (total magnification ×100).

Figure 6. Ovary, postnatal day 21, Vantex group. Ki-67-positive parenchymal and stromal cells (1). Immunohistochemistry, DAB chromogen with haematoxylin counterstain; objective ×20 (total magnification ×200).

Figure 7. Ovary, postnatal day 30, Vantex group. Bcl-2-positive expression (1). Immunohistochemistry, DAB chromogen with haematoxylin counterstain; objective ×40 (total magnification ×400).

Figure 8. Quantitative statements reported for this experimental model. (A) Ovarian medullary venule lumen at postnatal day 21, expressed as fold change relative to intact controls [1]. (B) Physiological expansion of the uterine venous bed in control offspring at postnatal day 30 relative to early postnatal life [2]; this expansion is blunted after maternal exposure, but the source does not quantify the shortfall. Panels A and B answer different questions and must not be read as a single comparison. No value in this figure was measured for the present article.

Figure 9. Semi-quantitative severity profile of the Vantex group. (A) Summed scores for six exudative–congestive features and for seven sclerotic–ischaemic and parenchymal features across postnatal days 7–30; the trajectories cross between postnatal days 14 and 21. (B) The underlying score matrix (0 = absent, 1 = mild, 2 = moderate, 3 = marked); the rule separates the two feature groups. Scores are an ordinal summary of the qualitative observations assigned by the author, not measurements, and were not tested statistically. The full scoring sheet, with the wording of the source text on which each score rests, is provided in the accompanying data workbook.

Figure 10. Proposed pathogenetic sequence linking chronic maternal Vantex exposure to disturbed postnatal utero-ovarian morphogenesis. This is a schematic concept diagram summarising the interpretation presented in Sections 3 and 4; it is not derived from measured data and expresses no quantitative claim. The ratio shown for postnatal day 21 is the directional value reported in [1].

Figures 2–7 are photomicrographs from the author's experimental series, recovered from the original image files and cropped without any adjustment of tone, contrast, colour or local content; they were resampled with a Lanczos filter for print output at 300 dpi. No feature was enhanced, obscured, moved or introduced. Calibrated scale bars were not recorded at image acquisition, so magnification is reported throughout as the objective–ocular combination together with the resulting total magnification.

Ilova A. Annotatsiya (o‘zbek tilida)

Maqsad. Vanteks pestitsidining ona organizmiga surunkali past dozali toksik ta’siri sharoitida naslda bachadon va tuxumdon gemomikrosirkulyator o‘zani hamda to‘qima tuzilmalarining postnatal morfogenezini o‘rganish; proliferatsiya (Ki-67) va antiapoptotik (Bcl-2) immunoreaktivlikni baholash. Material va usullar. Oq naslsiz kalamushlar ikki guruhga ajratildi (har birida 30 ta ona): nazorat va tajriba. Tajriba guruhidagi onalarga Vanteks 4,0 mg/kg/kun miqdorida teri orqali, homiladorlik va laktatsiya davrida yuborildi. Nasl tug‘ruqdan keyingi 7-, 14-, 21- va 30-kunlarda tekshirildi. Bachadon angioarxitektonikasi qorin aortasi orqali Gerota massasi yuborilgandan so‘ng Sagatov usulida tiniqlashtirish yo‘li bilan o‘rganildi; 5–7 μm kesmalar gematoksilin-eozin bilan bo‘yaldi; Ki-67 va Bcl-2 Ventana BenchMark XT tizimida DAB xromogeni yordamida aniqlandi. Baholash sifat va yarim miqdoriy tarzda olib borildi; statistik tahlil qo‘llanilmadi. Natijalar. Onaning Vanteks bilan surunkali zaharlanishi nasl reproduktiv a’zolarida yallig‘lanish-destruktiv tomir–to‘qima o‘zgarishlari, stromada kollagen va elastik tolalarning zichlashuvi, follikulalar markazidagi tuxum hujayralarining muddatidan oldin atreziyaga uchrashi, teka hujayralari distrofiyasi, lyuteotsitlarda nekroz o‘choqlari hamda bachadon vena o‘zanining fiziologik kengayishi susayishiga olib keldi. 21-kunga kelib mag‘iz qavat venulalari bo‘shlig‘i nazoratga nisbatan taxminan 1,3 barobar kengaydi. Ki-67 ifodasi istmikoservikal bezlarda hamda tuxumdon parenximasi va stromasida kuchaydi; Bcl-2 30-kunda ham aniq musbat bo‘lib qoldi. Tomir o‘zgarishlari parenxima shikastlanishidan oldin aniqlandi. Xulosa. Ushbu ona–nasl modelida Vanteks reproduktiv toksik xususiyatga ega bo‘lib, to‘qima shikastlanishi bevosita gemomikrosirkulyator o‘zan holatiga bog‘liq. Surunkali piretroid ta’siri ostidagi aholi uchun perinatal profilaktika choralari zarur.

Приложение В. Аннотация (на русском языке)

Цель. Изучить постнатальный морфогенез гемомикроциркуляторного русла и тканевых структур матки и яичников у потомства при хронической низкодозовой интоксикации матери пестицидом Вантекс; оценить экспрессию Ki-67 и Bcl-2. Материал и методы. Белые беспородные крысы, две группы по 30 матерей; Вантекс 4,0 мг/кг/сут накожно на протяжении беременности и лактации; сроки исследования — 7, 14, 21 и 30-е сутки постнатального развития; гематоксилин-эозин; ангиоархитектоника по Сагатову; иммуногистохимия на Ventana BenchMark XT. Статистический анализ не проводился. Результаты. Воспалительно-деструктивная перестройка сосудов, уплотнение стромальных волокон, атрезия фолликулов, дистрофия теки, некроз лютеоцитов; просвет мозговых венул к 21-м суткам шире контроля примерно в 1,3 раза; усиление экспрессии Ki-67 и сохранение Bcl-2 к 30-м суткам. Вывод. Вантекс обладает свойствами репродуктивного токсиканта; тяжесть тканевых изменений определяется состоянием микроциркуляторного русла.